Materials and Design 60 (2014) 653–660

Contents lists available at ScienceDirect

Materials and Design

journal homepage: www.elsevier.com/locate/matdes

Crystallographic texture evolution in Ti–35Nb alloy deformed by cold rolling

Alexandra O.F. Hayama [a], Juliana F.S.C. Lopes [b], Marcelo J. Gomes da Silva [c], Hamilton F.G. Abreu [c], Rubens Caram [b,*]

[a] Federal University of Mato Grosso, Rondonópolis, MT, Brazil
[b] University of Campinas, Campinas, SP, Brazil
[c] Federal University of Ceará, Fortaleza, CE, Brazil

ARTICLE INFO

Article history:
Received 28 January 2014
Accepted 8 April 2014
Available online 16 April 2014

Keywords:
Ti alloys
Plastic deformation
Young's modulus
Crystallographic texture
Orientation relationship

ABSTRACT

This work presents the results of a microstructural characterization of the Ti–35Nb alloy deformed by cold rolling. Initially, samples of the Ti–35Nb (wt%) alloy were obtained by electric arc melting. After melting, these samples were solution heat-treated at 1000 °C for 8 h and water quenched. The resulting microstructure was composed of β-phase (bcc) combined with orthorhombic martensite (α″). Samples were cold-rolled in multiple passes to reduce their thickness by up to 85% without intermediary annealing. They were then characterized by light optical microscopy, X-ray diffraction and Vickers hardness measurements. Young's modulus was determined by ultrasonic methods and nanoindentation measurements. The texture evolution and orientation relationship between phases were studied by X-ray diffraction and electron backscatter diffraction (EBSD). The results reveal the presence of shear bands in the deformed samples, an orientation of the orthorhombic martensite phase in relation to the rolling direction, and variations of Young's modulus in response to deformation. The textural results of the β-phase show a typical bcc rolling texture with strong (1 1 0) fiber and weak (1 1 1) fiber. The intensity of the (1 1 0) fiber increases with deformation.

1. Introduction

Titanium alloys present interesting combinations of mechanical and physical properties, including high strength-to-weight ratios and excellent corrosion resistance [1,2]. Due to their characteristics, these materials are used for a variety of applications in the chemical, biomedical and nuclear industries. The most suitable properties for each application are obtained by a combination of microstructures, which result from phase transformations in these alloys.

Titanium alloys can be classified into three groups: α alloys, α + β alloys and β alloys. The Ti–6Al–4V alloy, the main representative of α + β alloys, has long been used extensively in the production of orthopedic implants, replacing commercially pure titanium. This widespread use is attributed to its interesting properties, which include high mechanical strength. New alloys are being developed to replace the Ti–6Al–4V alloy in orthopedic implants [3]. Vanadium is considered toxic and a potential danger to the health of people with these implants [4]. Aluminum can also be harmful, causing localized inflammation [5], and may also be related to neurological disorders [6]. As a result, β titanium alloys have become alternative materials for the production of orthopedic implants [7]. Orthopedic β titanium alloys are obtained from biocompatible, nontoxic elements such as niobium, zirconium and tantalum and may present a lower Young's modulus than that of α + β alloy. Structural biomaterials employed as orthopedic devices must present an elastic modulus similar to that of bone (cortical bone is only about 17 GPa) [8]. In the case of β titanium alloys, this modulus may be as low as 50 GPa [9]. In addition, materials used in permanent implants in the human body must exhibit biocompatibility and corrosion resistance to provide osseointegration and biofunctionality [10].

β titanium alloys have the potential to replace α + β alloys in the manufacture of orthopedic implants in the near future. This fact has been stimulating research on the mechanisms and parameters of influence involved in the definition of the microstructure of these alloys, leading to the development of materials with ideal behavior for orthopedic applications. The rapid cooling of solution heat-treated β titanium alloys in the β field results in

* Corresponding author. Address: Rua Mendeleiev, 200, 13083-860 Campinas, SP, Brazil. Tel.: +55 19 3521 3314; fax: +55 19 3289 3722.
E-mail address: caram@fem.unicamp.br (R. Caram).

http://dx.doi.org/10.1016/j.matdes.2014.04.024
0261-3069/

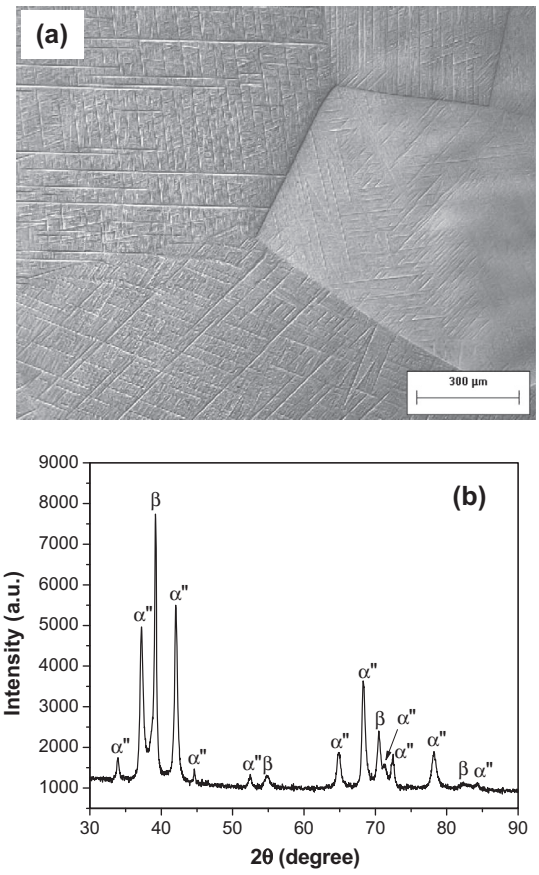

Fig. 1. The Ti–35Nb alloy in the solution heat-treated condition: (a) Microstructure (LOM – Nomarski contrast); (b) X-ray diffraction patterns.

Table 1
Vickers micro- and nanohardness and Young's modulus measured by the ultrasonic technique (UT) and nanoindentation of a sample of the solution condition.

E (GPa) ultrasound	E (GPa) nanoindentation	VHN microindentation	VHN nanoindentation
65 ± 1	63 ± 3	181 ± 4	194 ± 6

microstructures composed of martensitic and β phases [11]. These phases usually present low values of Young's modulus and mechanical strength. However, the application of aging heat treatment at intermediate temperatures can improve their mechanical behavior by promoting phase transformation and replacing the previous microstructure with a combination of α and β phases [12]. In β titanium alloys, the effect of plastic deformation on phase transformations during aging heat treatments is not well known. It is possible that deformation produced by cold rolling can play an important role in the way α phase is precipitated, and hence, may alter the phase distribution and final microstructure.

This paper discusses the effect of plastic deformation on the microstructural evolution of β Ti–Nb subjected to aging heat treatment and analyzes the texture evolution and orientation relationship between phases.

2. Experimental details

The starting material was obtained by electric arc melting, then sealed in quartz glass and solution heat-treated at 1000 °C for 8 h, followed by quenching in water at room temperature. The resulting microstructure was composed of β phase and orthorhombic martensite (α″). Solution heat-treated samples were deformed by cold rolling in multiple passes, which reduced their thickness by up to 85% without requiring intermediary annealing. At each deformation pass, a sample was removed for characterization. In this paper, the acronym RD indicates the rolling direction, TD indicates the transverse direction and ND indicates the normal direction of the rolled sheet. Specimens were cut out parallel to the RD. The samples were prepared for metallographic analysis with a solution composed of 260 mL of OP-S, 1 mL of HNO_3 and 0.5 mL of HF. The microstructure was revealed with a metallographic etchant composed of H_2O, HF and HNO_3, in a proportion of 85:10:5 (in volume); etching time varied from 10 to 20 s.

The material was characterized by X-ray diffraction, Vickers microhardness, light optical microscopy (LOM), ultrasonic techniques (US), nanoindentation measurements and analyses of nitrogen and oxygen. X-ray diffraction measurements were taken using Cu Kα radiation in a PANalytical X'Pert PRO diffractometer. Vickers microhardness tests were carried out on polished samples in the solution heat-treated and deformed conditions, applying a load of 100 g on their transverse section. The microstructures of initial and deformed samples were examined under an Olympus BX60M light optical microscope (LOM) equipped with a digital camera for image acquisition (Evolution LC Color) coupled to image analyzer software (Materials-Pro). Young's modulus (E) was determined by ultrasonic techniques (US) and measurements were taken with a Panametrics-NDT 5072PR pulser-receiver with 5 MHz transducers. A coupling material was placed between the transducer and the sample. Nanoindentation measurements used for the determination of Young's modulus were taken with a CSM Instruments Nanoindentation Tester under a load of 100 mN. Oxygen and nitrogen were analyzed in a LECO TC400 gas analyzer.

Texture was examined in a Philips XPRO X-ray diffractometer (XRD) with Cu Kα radiation. XRD was used to measure three incomplete pole figures (110), (211) and (222) of the β phase and (200) and (131) of the α″ phase. Pole figures were measured using a maximum tilt of 80° on the central layer of the sheet. Orientation distribution functions (ODF) were calculated for these three pole figures of the β phase using the ADC method with Labotex software. An HKL Channel 5 system attached to a Philips XL-30 scanning electron microscope was used for orientation relation studies.

3. Results and discussion

3.1. Solution heat-treated condition

The oxygen and nitrogen content of the Ti–35Nb samples in the solution heat-treated condition were 0.111 wt% and 0.0155 wt%, respectively. These interstitial contents are in agreement with the ASTM: B-348-13 standard. The microstructure of the Ti–35Nb samples consisted of coarse grains with a diameter of approximately 3 mm (Fig. 1a). The samples in this condition showed a high volumetric fraction of orthorhombic martensite (α″).

Fig. 1b shows XRD patterns of the Ti–35Nb alloy in the solution heat-treated condition. Peaks of β and α″ phases were identified. Rapid quenching from temperatures in the β field of Ti alloys with large amounts of β-stabilizing elements resulted in the formation of orthorhombic martensite α″ and stabilization of the β phase. The minimum amount of β-stabilizer element needed to complete retain the β phase (metastable β) is 36 wt% Nb [13]. This may explain the amount of martensite observed in the microstructure.

Table 1 shows the results of Vickers micro- and nanohardness and of Young's modulus measured by the ultrasonic and nanoindentation techniques. The hardness and Young's modulus results

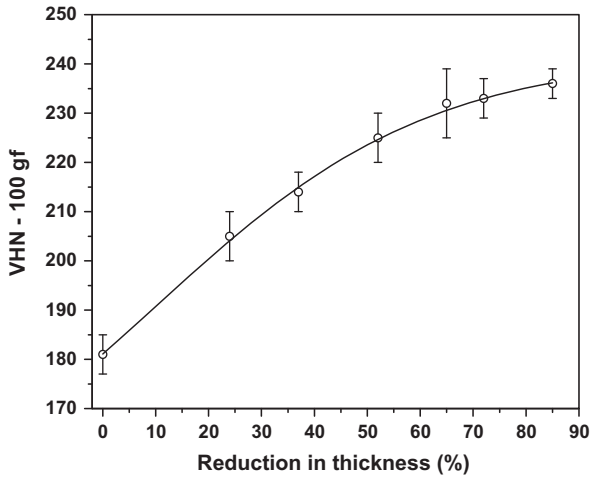

Fig. 2. Work-hardening behavior of the Ti–35Nb alloy during cold rolling.

obtained by these two techniques showed a good consistency. Ozaki et al. [13] studied alloys in the Ti–Nb system and found that the lowest values of Young's modulus in the range of compositions between 15 and 42 wt%–Nb were obtained after a solution heat-treatment. The Young's modulus they determined was approximately equal to 70 GPa for solution heat-treated samples of the Ti–35Nb alloy and is similar to that obtained in this work.

3.2. Deformed specimens

In the solution heat-treated condition, the Ti–35Nb alloy is highly ductile and can be rolled to very large strains at room temperature. In this work, we successfully deformed the Ti–35Nb alloy up to 85% by cold rolling. Samples corresponding to thickness reductions varying from 24% to 85% were obtained. Fig. 2 shows the work-hardening behavior of the Ti–35Nb alloy deformed by cold rolling. A tendency for saturation was observed when the thickness reduction exceeded 72%.

The microstructure of the Ti–35Nb alloy after cold rolling was characterized by light optical microscopy, using preferentially the Nomarski contrast technique to accentuate the relief of the samples. Generally speaking, the samples presented deformation heterogeneities, such as shear bands, which occurred in more strongly deformed samples.

An observation of the Ti–35Nb alloy microstructure indicates that the subdivision of grains during plastic deformation varied from one grain to another, and was characterized by different

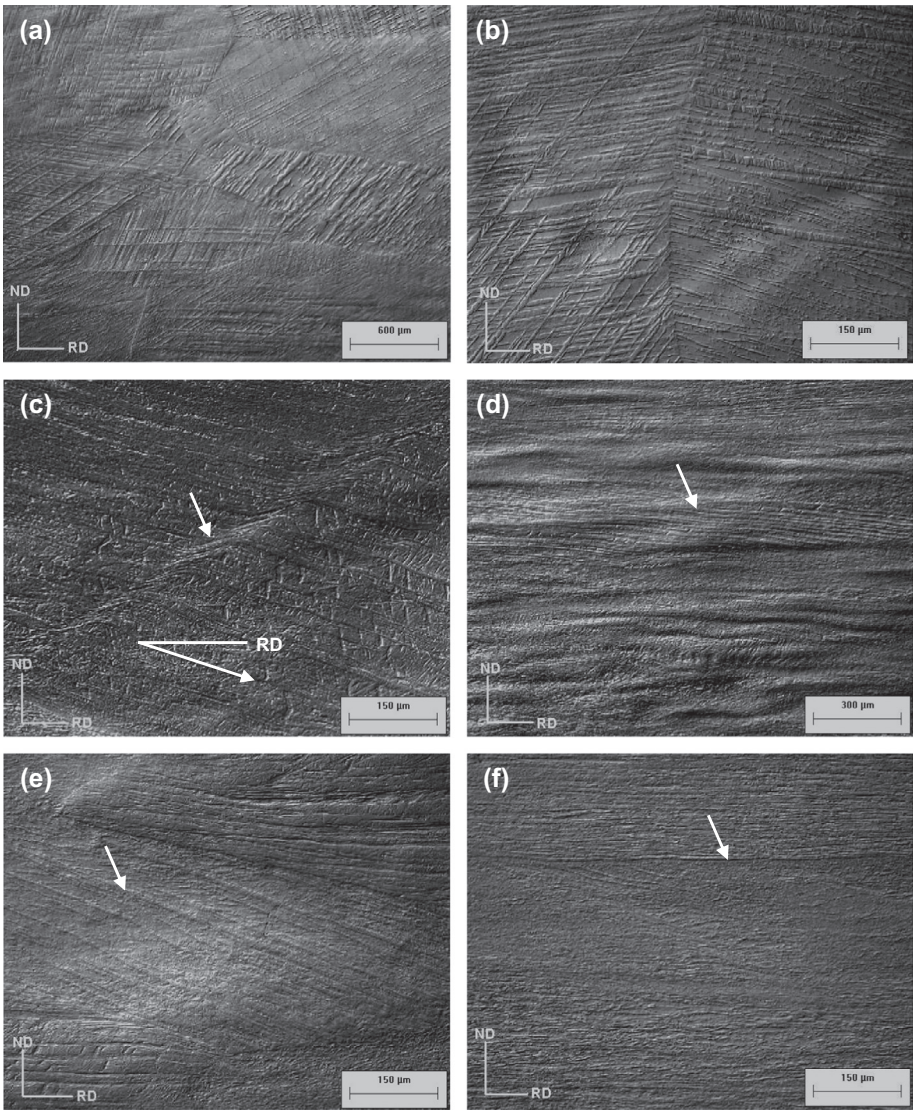

Fig. 3. Microstructures of the Ti–35Nb alloy deformed up to: (a) 24%, (b) 37%, (c) 52%, (d) 65%, (e) 72%, and (f) 85% (LOM – Nomarski contrast).

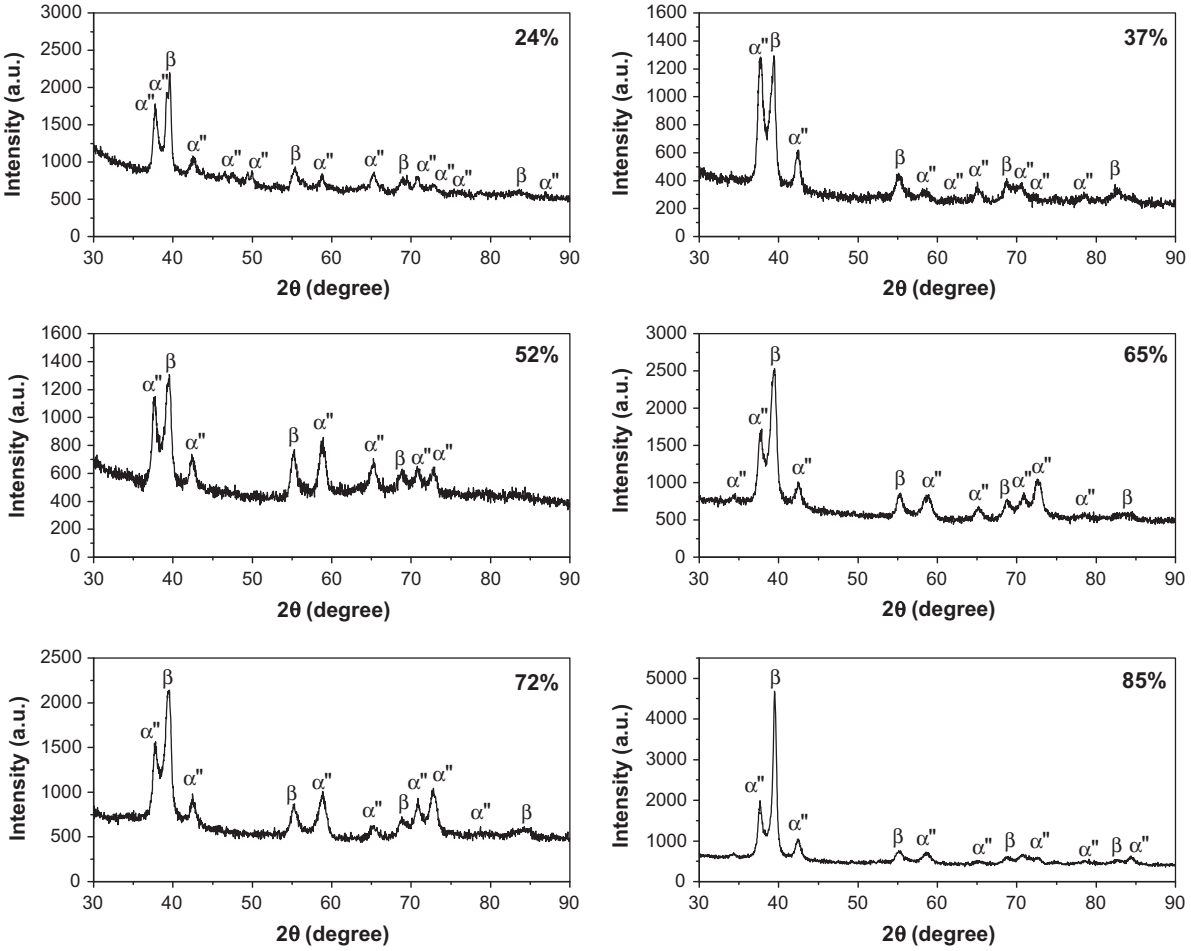

Fig. 4. X-ray diffraction patterns analyzed on a rolling plane of the Ti–35Nb alloy as a function of cold rolling.

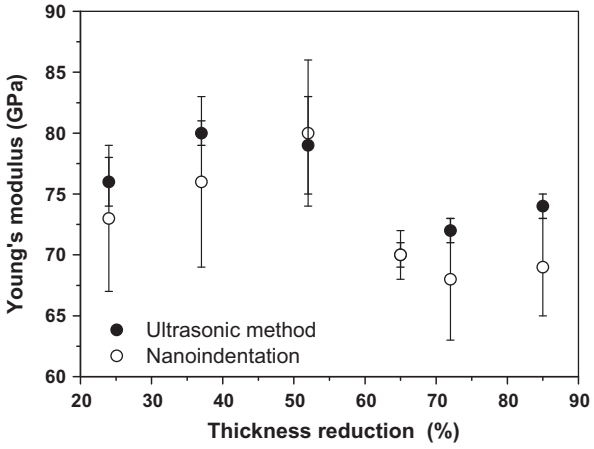

Fig. 5. Young's modulus determined by ultrasonic methods and nanoindentation measurements of samples of the Ti–35Nb alloy deformed up to 85%.

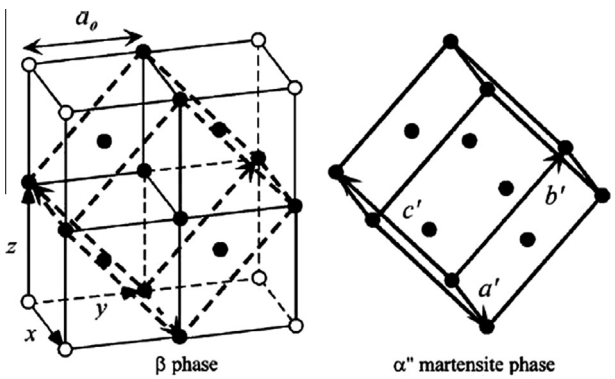

Fig. 6. Correspondence between β and α″ phases [16].

volume fractions of the α″ phase induced by deformation inside the grains. This characteristic is illustrated in Fig. 3a and b, which shows the microstructure of samples with 24% and 37% thickness reduction, respectively. In these samples, alignments of the α″ phase in relation to the rolling direction were also verified.

Higher plastic deformations of up to 52% led to deformation heterogeneities and the microstruture became lamellar, with boundaries aligned parallel to the rolling direction (Fig. 3c). At very high strains (above 52%), deformation heterogeneities appeared in the microstructure to accommodate the increasing strain in the Ti–35Nb alloy, especially shear bands. These bands formed angles of 30–35° with the RD. Fig. 3c and f shows the presence of shear bands in the microstructure. These bands are important deformation heterogeneities which act as preferential nucleation sites for

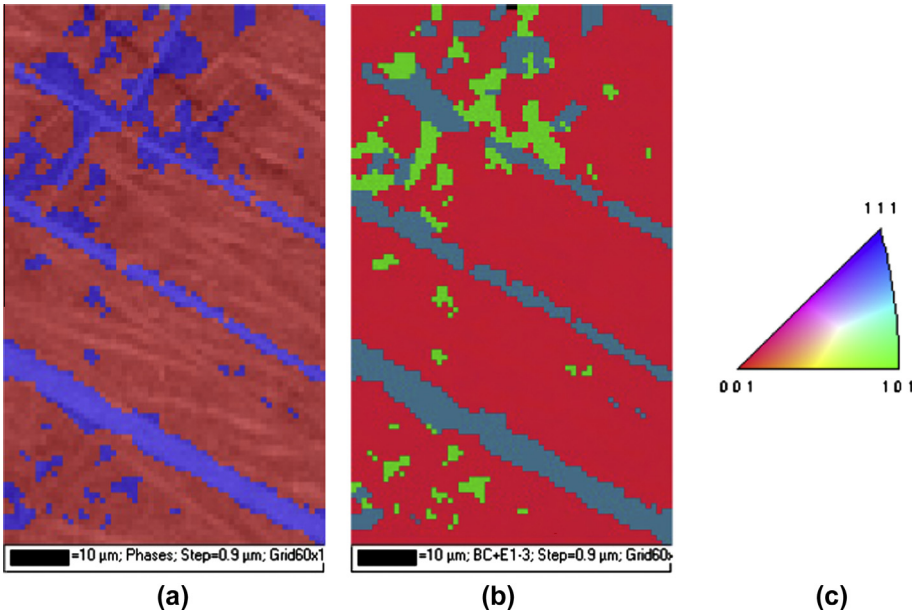

Fig. 7. The Ti–35Nb alloy deformed up to 85%: (a) EBSD phase map; (b) orientation distribution map. The unit triangle with a color scheme to guide the eye is also indicated.

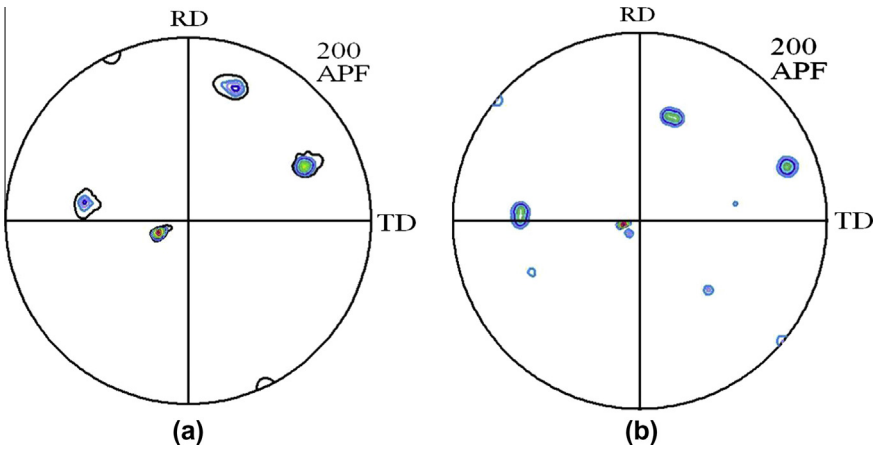

Fig. 8. (200) pole figure of the martensite phase: (a) measured by EBSD; (b) calculated.

recrystallization when the previously deformed material is subjected to high temperatures [14].

Fig. 4 shows XRD patterns of the Ti–35Nb alloy deformed by cold rolling. This diffractogram shows diffraction peaks of β and α″ phases. The intensities of the β phase diffraction peaks did not change significantly in response to rolling reduction, suggesting that the amount of the orthorhombic phase does not increase significantly with deformation. Matsumoto et al. [15] observed a similar behavior in their study of the Ti–35Nb–4Sn (wt%) alloy. They also observed that a different type of martensite texture becomes predominant during cold plastic deformation.

Young's modulus of the deformed samples was determined by the ultrasonic method and from nanoindentation measurements. Fig. 5 shows the variation of Young's modulus with the increase in deformation by cold rolling. The results obtained by the two techniques are in good agreement. In the deformed samples, a variation was noted in the values of Young's modulus, which increased in samples deformed to 52% and decreased in samples deformed to 85%. Matsumoto et al. [15] also reported a variation in Young's modulus in the Ti–35Nb–4Sn (wt%) alloy. They found that Young's modulus increased slightly at 30% rolling reduction and decreased as this reduction increased from 50 to 89% and according to them, these changes may be connected with martensite texture due to stress-induced martensitic phase transformation. They suggested that a decrease in Young's modulus is due to the development of $(200)_{\alpha''}/[010]_{\alpha''}$ texture, while an increase may be a result of the development of texture of other than $(200)_{\alpha''}/[010]_{\alpha''}$.

Martensite in Ti–Nb alloys changes from a hexagonal to an orthorhombic crystal structure as the Nb content increases [16,17]. Water quenched Ti–35Nb (wt%) alloy exhibits a martensitic transformation from β (body-centered cubic) to orthorhombic (α″) martensite. The schematic illustration in Fig. 6 shows a lattice correspondence between β and α″ phases. Kim et al. [18] measured the lattice constants of the β and α″ phases in the Ti–35Nb at room temperature and found for cubic $a_0 = 0.329$ nm and for orthorhombic α″, respectively, $a' = 0.317$ nm, $b' = 0.4809$ nm and $c' = 0.466$ nm. The space group of the orthorhombic phase is CMCM (63).

The orientation relationship proposed by Kim et al. [18] to relate β phase and α″ orthorhombic phase is:

$$[100]_{\alpha''}//[100]_{\beta} \quad [010]_{\alpha''}//[011]_{\beta} \quad [001]_{\alpha''}//[0\bar{1}1]_{\beta}$$

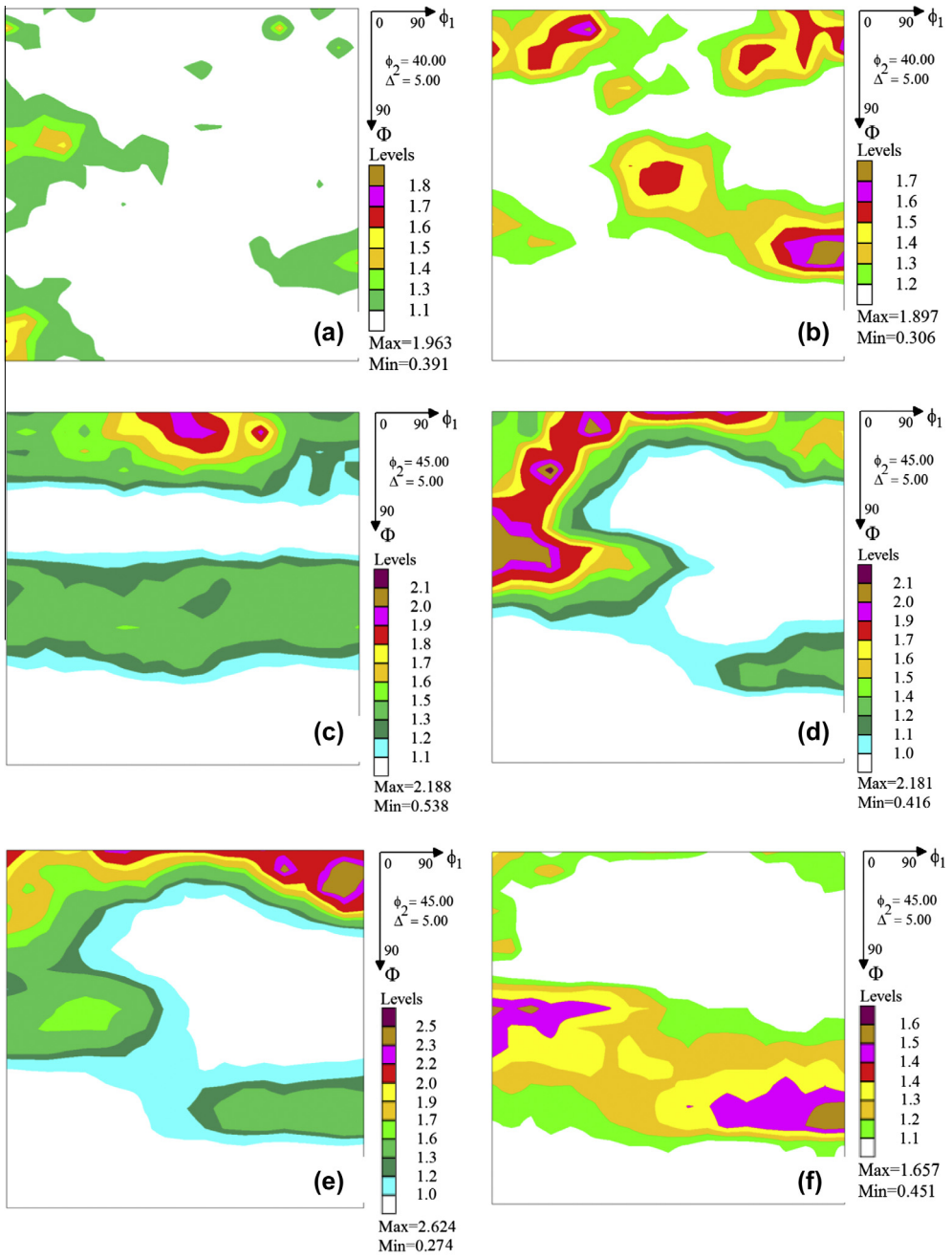

Fig. 9. Bunge 45° ODF sections analyzed on the rolling plane of samples of the Ti–35Nb alloy cold rolled up to: (a) 24%, (b) 37%, (c) 52%, (d) 65%, (e) 72%, and (f) 85%.

The deformation matrix representing $\beta \rightarrow \alpha''$ proposed by Kim et al. [18] is:

$$(\beta S \beta) = \begin{pmatrix} a'/a_0 & 0 & 0 \\ 0 & b' + c'/2\sqrt{2}a_0 & b' - c'/2\sqrt{2}a_0 \\ 0 & b' - c'/2\sqrt{2}a_0 & b' + c'/2\sqrt{2}a_0 \end{pmatrix} = \begin{pmatrix} 0.9635 & 0 & 0 \\ 0 & 0.9835 & 0.0155 \\ 0 & 0.0155 & 0.9835 \end{pmatrix} \quad (1)$$

The correspondence matrix obtained by observation of Fig. 6 is [18]:

$$(\alpha'' C \beta) = \begin{pmatrix} 1 & 0 & 0 \\ 0 & 2 & 2 \\ 0 & \bar{2} & 2 \end{pmatrix} \quad (2)$$

Following the procedure described in reference [19], we calculated the coordinate transformation matrix (α'' J β) using the equation:

$$(\alpha'' J \beta) = (\alpha'' C \beta)(\beta S \beta)^{-1} \quad (3)$$

$$(\alpha'' J \beta) = \begin{pmatrix} 1.0379 & 0 & 0 \\ 0 & 1.9370 & 1.9370 \\ 0 & -1.9970 & 1.9970 \end{pmatrix} \quad (4)$$

Fig. 7a and b shows, respectively, the EBSD phase map and orientation distribution map for the two phases (α'' and β). The red area in both figures corresponds to β-phase. The total area studied by EBSD is confined in the same β grain and its orientation is defined by Euler angles $\varphi_1 = 336°$, $\phi = 20°$ and $\varphi_2 = 41°$. The

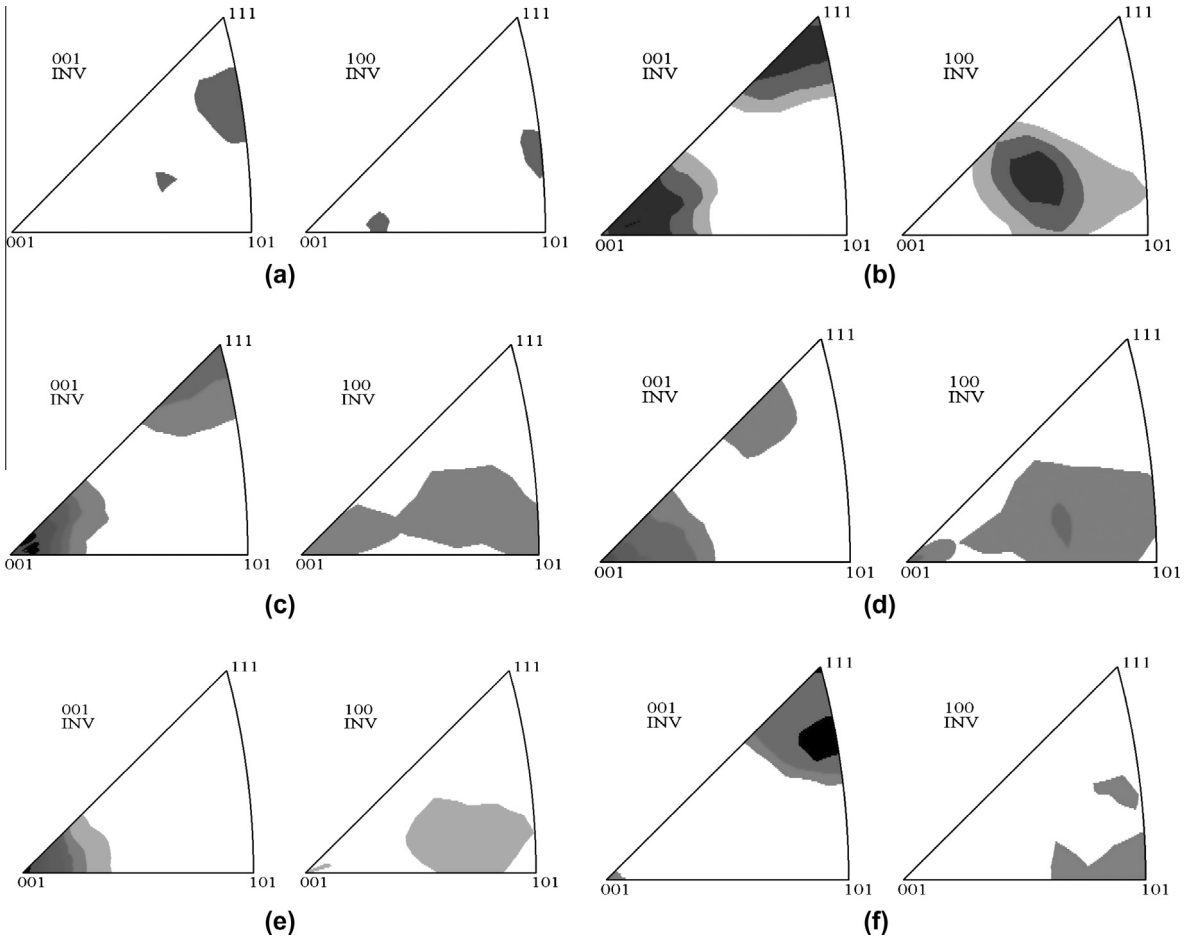

Fig. 10. IPF analyzed on the rolling plane of samples of the Ti–35Nb alloy cold rolled up to: (a) 24%, (b) 37%, (c) 52%, (d) 65%, (e) 72%, and (f) 85%.

orientation map shows two different variants for the martensite phase. Fig. 8a shows the (200) pole figure for martensite phase. Fig. 8b is the (200) pole figure calculated with the matrix (α″ J β) and assuming that 4 variants would be present after transformation. The calculated and measured pole figures show a slight difference in misorientation, but the calculated coordinate transformation matrix (α″ J β) appears to be a good approximation to the transformation matrix from β-bcc to α″-orthorhombic. The calculated pole figure contains more poles than the measured one. This is due to variant selection, which is more intense than that proposed in the model.

One possibility for using these alloys is after they have undergone a cold rolling process. It is therefore important to study the evolution of the texture in response to deformation. Raabe et al. [20] studied texture evolution in the β phase (body-centered cubic) during rolling of several Ti–Nb compositions. They reported that these alloys showed a typical bcc rolling texture with a strong alpha fiber and a weak gamma fiber [19].

In the present work, the evolution of crystallographic texture in the β phase was evaluated by X-ray diffraction and the variations in the Young's modulus were attributed to the development of β phase texture during the cold rolling of this alloy. Figs. 9 and 10 show the ODF (Orientation Distribution Function) and IPF (Inverse Pole Figure), respectively, analyzed in the rolling plane of the Ti–35Nb alloy subjected to cold rolling varying from 24% to 85%. The IPF shows how the selected direction in the sample's reference frame is distributed in the reference frame of the crystal. In these figures, ⟨001⟩ corresponds to ND and ⟨100⟩ to RD.

The rolling texture of many bcc materials is characterized by two crystallographic fibers, the α-fiber with ⟨011⟩//RD and the γ-fiber with {111}//ND. The texture of the 24% deformed sample is very weak. Increasing the deformation to 37% and 52% of thickness reduction causes the formation of γ and α fibers, but the most intense component in these samples is between {001}⟨100⟩ and {001}⟨110⟩. Samples deformed to 65% (Figs. 9d and 10d) and 72% (Figs. 9e and 10e) present texture components {001}⟨110⟩, {112}⟨110⟩ and {111}⟨101⟩. The sample deformed up to 85% presents a reduction in component {001}⟨110⟩ and an increase in the intensity of component {111}⟨101⟩. The evolution of the rolling texture of these alloys is more evident in Fig. 10 that shows the sequence of IPF's from 24% deformed to 85% deformed.

The texture analysis of the orthorhombic phase involved the analysis of pole figures (200) and (131), which were the only ones with sufficient intensity to measure pole figures in all the stages of plastic deformation. Fig. 11 shows the α″ rolling texture drawn by (200) and (131) pole figures obtained in the rolling plane as a function of rolling reduction. Pole figures from samples deformed by more than 65% show components $\{1\bar{2}1\}$ $\langle\bar{2}14\rangle$ and $\{1\bar{4}2\}$ $\langle\bar{2}13\rangle$.

4. Conclusions

The Ti–35Nb samples were obtained by electric arc melting, solution heat-treated, followed by quenching in water at room temperature. The resulting microstructure was composed of β phase and orthorhombic martensite (α″). These samples were deformed by cold rolling in multiple passes, which reduced their thickness by up to 85% without requiring intermediary annealing. The microstructural characterization of samples in the deformed

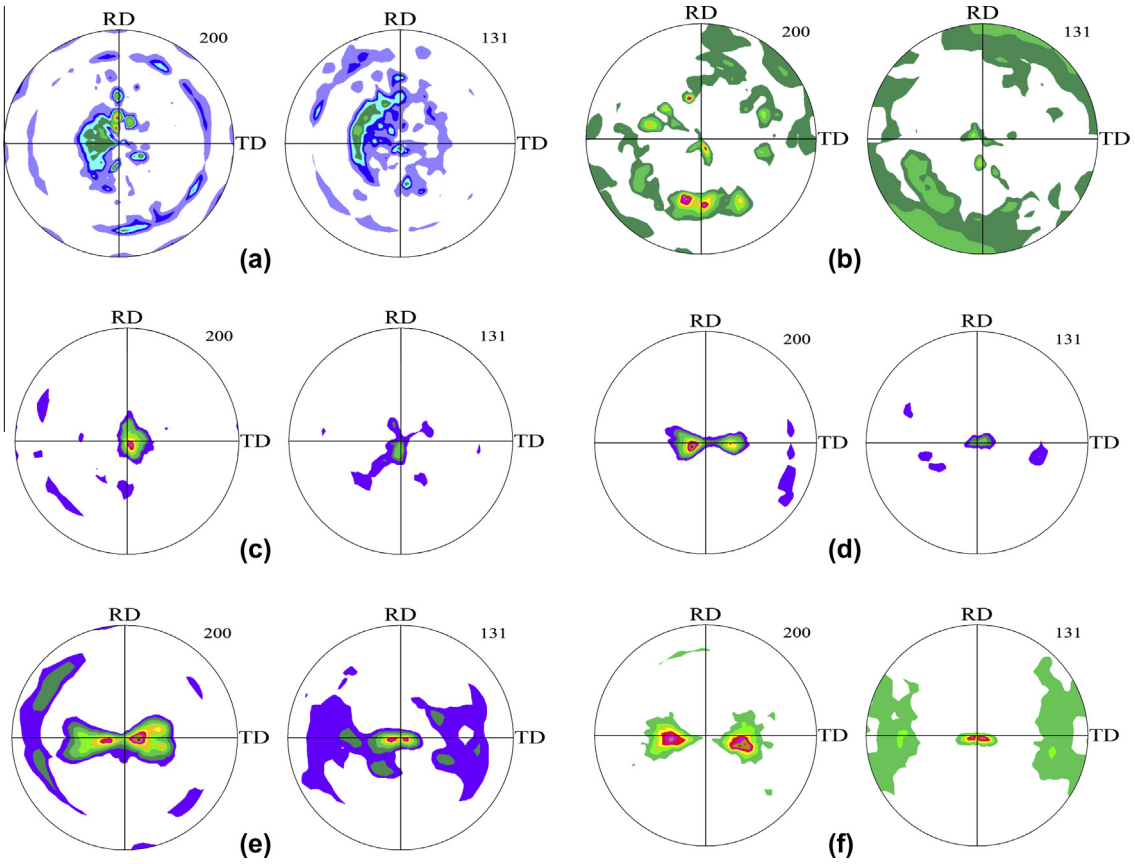

Fig. 11. PF analyzed in rolling plane for samples of the Ti–35Nb alloy cold rolled up to: (a) 24%, (b) 37%, (c) 52%, (d) 65%, (e) 72%, and (f) 85%.

condition indicated that the martensite phase (α″) tended to align with the rolling direction in less deformed samples (deformation up to 37%). Moreover, the deformation process led to deformation heterogeneities such as shear bands. The deformed samples also showed a change in Young's modulus, i.e., samples deformed between 22% and 52% showed an increase in the elastic modulus. The elastic modulus decreased in response to deformation exceeding 52%. This behavior may be attributed to the development of β texture during the cold rolling of this alloy. The textural results of the β-phase show a typical bcc rolling texture with strong (1 1 0) fiber and weak (1 1 1) fiber. The intensity of the (1 1 0) fiber increases with deformation.

Acknowledgements

The authors gratefully acknowledge the Brazilian research funding agencies FAPESP (State of São Paulo Research Foundation), CNPq (National Council for Scientific and Technological Development) and CAPES (Federal Agency for the support and Evaluation of Graduate Education) for their financial support of this work.

References

[1] Lütjering G, Williams JC. Titanium. Berlin: Springer; 2003.
[2] Cui C, Hu B, Zhao L, Liu S. Titanium alloy production technology, market prospects and industry development. Mater Des 2011;32:1684–91.
[3] Slokar L, Matković T, Matković P. Alloy design and property evaluation of new Ti–Cr–Nb alloys. Mater Des 2012;33:26–30.
[4] Eisenbarth E, Velten D, Müller M, Thull R, Breme J. Biocompatibility of β-stabilizing elements of titanium alloys. Biomaterials 2004;25:5705–13.
[5] Zaffe D, Bertoldi C, Consolo U. Accumulation of aluminum in lamellar bone after implantation of titanium plates, Ti–6Al–4V screws, hydroxyapatite granules. Biomaterials 2004;25:3837–44.
[6] Silva HM, Schneider SG, Moura Neto C. Study of nontoxic aluminum and vanadium-free titanium alloys for biomedical applications. Mater Sci Eng C 2004;24:679–82.
[7] Guo Q, Zhan Y, Mo H, Zhang G. Aging response of the Ti–Nb system biomaterials with β-stabilizing elements. Mater Des 2010;31:4842–6.
[8] Yan W, Berthe J, Wen C. Numerical investigation of the effect of porous titanium femoral prosthesis on bone remodeling. Mater Des 2011;32:1776–82.
[9] Kuroda D, Niinomi M, Morinaga M, Kato Y, Yashiro T. Design and mechanical properties of new beta type titanium alloys for implant materials. Mater Sci Eng A 1998:243–6.
[10] Tamirisakandala S, Vedam BV, Bhat RB. Recent advances in the deformation processing of titanium alloys. J Mater Eng 2003;12:661–73.
[11] Cardoso FF, Ferrandini PL, Lopes ESN, Cremasco A, Caram R. Ti–Mo alloys employed as biomaterials: effects of composition and aging heat treatment on microstructure and mechanical behavior. J Mech Behav Biomed Mater 2014;32:31–8.
[12] Cremasco A, Andrade PN, Contieri RJ, Lopes ESN, Afonso CRM, Caram R. Correlations between aging heat treatment, ω phase precipitation and mechanical properties of a cast Ti–Nb alloy. Mater Des 2011;32:2387–90.
[13] Ozaki T, Matsumoto H, Watanabe S, Hanada S. Beta Ti alloys with low Young's modulus. Mater Trans 2004;45:2776–9.
[14] Humphreys FJ, Hatherly M. Recrystallization and Related Annealing Phenomena. Kidlington, UK: Elsevier; 2004.
[15] Matsumoto H, Watanabe S, Hanada S. Microstructures and mechanical properties of metastable β Ti–Nb–Sn alloys cold rolled and heat treated. J Alloy Compd 2007;439:146–55.
[16] Williams JC, Hickman BS. Tempering behavior of orthorhombic martensite in titanium alloys. Metall Mater Trans B 1970;1:2648–50.
[17] Lopes ESN, Cremasco A, Afonso CRM, Caram R. Effects of double aging heat treatment on the microstructure, Vickers hardness and elastic modulus of Ti–Nb alloys. Mater Charact 2011;62:673–80.
[18] Kim HY, Ikehara Y, Kim JI, Hosoda H, Miyazaki S. Martensitic transformation, shape memory effect and superelasticity of Ti–Nb binary alloys. Acta Mater 2006;54:2419–29.
[19] Bhadeshia HKDH. Geometry of Crystals, 2nd ed., Institute of Materials. 2001.
[20] Raabe D, Sander B, Friák M, Ma D, Neugebauer J. Theory-guided bottom-up design of β-titanium alloys as biomaterials based on first principles calculations: theory and experiments. Acta Mater 2007;55:4475–87.